

# Engineering and Tuning of high quality hexagonal boron nitride nanophotonic resonators

Otto Cranwell Schaeper<sup>1,2</sup>, Angus Gale<sup>1,\*</sup>, Nathan Coste<sup>1,2</sup>, Dominic Scognamiglio<sup>1</sup>, Jake Horder<sup>1</sup>, Hugo Quard<sup>1,2</sup>, Igor Aharonovich<sup>1,2,\*</sup>

<sup>1</sup> School of Mathematical and Physical Sciences, Faculty of Science, University of Technology Sydney, Ultimo, New South Wales 2007, Australia

<sup>2</sup> ARC Centre of Excellence for Transformative Meta-Optical Systems (TMOS), University of Technology Sydney, Ultimo, New South Wales 2007, Australia

\* [angus.gale@uts.edu.au](mailto:angus.gale@uts.edu.au), [igor.aharonovich@uts.edu.au](mailto:igor.aharonovich@uts.edu.au)

## Abstract

*Van der Waals materials are offering intriguing opportunities as building blocks for advanced quantum information technologies and integrated quantum photonic systems. Critical to their development, is robust and high quality light-matter interactions which can be delivered through the fabrication of optical resonators. Here we demonstrate a robust fabrication of one dimensional photonic crystal cavities (1D PCC) and microdisk resonators from hexagonal boron nitride, exhibiting Quality factors of  $\sim 4300$  and  $\sim 8300$ , respectively. With these two classes of devices we demonstrated cavity mode tuning via atomic layer deposition and gas condensation. Cavity resonances were shifted by and  $\sim 9$  nm for the 1D PCCs and  $\sim 16$  nm in the microdisk resonators, respectively. Our work opening a promising pathway for a realisation emitter – cavity coupling in hBN and eventually to a fully integrated quantum photonic circuitry with hBN.*

Integrated photonics is a key enabler for quantum information processing <sup>1, 2</sup>, sensing <sup>3</sup>, and communication <sup>4</sup>, enabling engineered light–matter interactions on-chip <sup>5-7</sup>. Across traditional three-dimensional platforms—including for example silicon, diamond, lithium niobate, - mature fabrication technologies have delivered high-performance cavities and waveguides <sup>8-12</sup>. Performance of these devices is often assessed by measuring their quality factors (Q) and striving to engineer geometries with the smallest mode volume (V) <sup>13-16</sup>.

Among explored cavity geometries, microdisk resonators support whispering-gallery modes (WGMs) with high Q and fields localized along the disk edge <sup>17, 18</sup>. These devices were often used to demonstrate strong coupling for ensembles of emitters and collective phenomena such as superradiance <sup>18, 19</sup>. Photonic crystal cavities (PCCs) offer lower mode volumes, thus making them attractive for quantum applications and coupling to single-photon sources <sup>13, 20, 21</sup>. PCCs typically support a single fundamental mode to maximize light–matter interaction with the embedded emitter. This, however, makes spectral alignment challenging due to fabrication variability of the PCCs and emitter wavelength dispersion. Consequently, post-fabrication tuning of cavity modes, for both microdisks and PCCs is therefore essential <sup>22-24</sup>.

In recent years, hexagonal boron nitride (hBN) has emerged as a promising material for integrated photonics <sup>25-30</sup>. It is transparent in the visible to near infrared and hosts a variety of ultra bright single-photon emitters and spin-active defects, some of which can be engineered on demand with nanoscale resolution<sup>31, 32</sup>. Furthermore, hBN’s van der Waals nature enables exfoliation into atomically smooth flakes of tunable thickness, supporting fabrication of

nanophotonic resonators and waveguides<sup>33</sup>. Due to the moderately low refractive index of hBN ( $n \sim 1.8$ )<sup>34</sup>, optical isolation through undercutting is critical, as substrate leakage severely degrades cavity performance.

In the current work, we report the design, fabrication, and characterization of hBN-based PCCs and microdisk resonators, specifically designed for the blue and the visible spectral range. We are particularly focused on developing a robust undercutting process that so far was challenging to achieve with hBN. Our devices exhibit high Quality factors of  $\sim Q \approx 4300$  at 578 nm for the PCCs, and  $Q \approx 8300$  at 460 nm for the microdisk cavities, respectively. Further, we demonstrate cavity mode tuning for both types of resonators via gas condensation and atomic layer deposition (ALD). These results pave the way for precise and reproducible spectral control of cavity modes in hBN devices—an essential step toward deterministic emitter–cavity coupling for scalable quantum photonic architectures.

Figure 1a shows a schematic illustration of the microdisk resonator and one dimensional (1D) PCC that are engineered and discussed in our work. The fabrication details are discussed in methods. Briefly, hBN was exfoliated onto silicon substrates, followed by patterning of the photonic structures using electron beam lithography (EBL) and a dry reactive ion etching. The fabricated structures were then suspended by undercutting the silicon in a potassium hydroxide (KOH) solution.

Figure 1(b-d) shows scanning electron microscope (SEM) images of the fabricated devices. Figure 1b displays two hBN microdisk resonators, sitting on a silicon pedestal. The surrounding hBN flake was inadvertently removed during the undercutting and drying process, but this has no effect on the efficacy of the device. Figures 1(c, d) display SEM images of 1D PCCs from different viewing angles, top down and tilted to 45 degrees, respectively. The 1D PCC features grating couplers to assist with the characterisation of the devices. The anisotropic nature of the silicon wet etch is clearly visible. Fabricated devices were aligned to ensure the etch would be deepest along the span of the cavity.

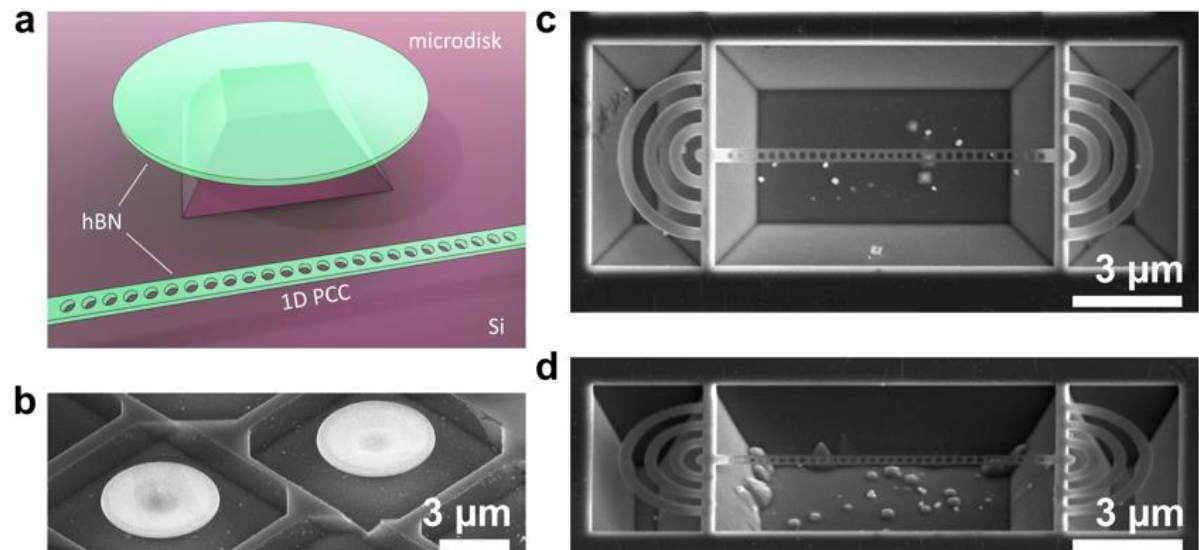


**Figure 1.** Overview of the fabricated cavity designs. a) Schematic of the two monolithic cavity designs fabricated from hBN, namely a microdisk resonator and 1D photonic crystal cavity (PCC). The silicon substrate is etched to undercut the cavities. b) SEM image of 5  $\mu\text{m}$  diameter

*hBN microdisks on silicon pedestals. c, d) SEM images of 1D PCCs integrated with grating couplers fabricated entirely from hBN. Top down and tilted to 45° angle, respectively.*

Figure 2(a,b) displays the Finite Difference Time Domain (FDTD) simulation of the cavity mode profiles simulated cavity. The mode confinement of 1D PCC is shown in two planes, (XY and XZ), respectively, with the cavity mode being confined to the central region of the device. The device characterisation was done using two complementary techniques. First, employing a standard photoluminescence (PL) measurement by confocal excitation and collection with a 532nm laser at the centre of the cavity. Second, by probing the cavity mode with resonant light: a broad laser pulse from a supercontinuum laser excites the cavity mode through a grating coupler, and the signal is collected from the top of the cavity. The excitation is polarized at a 45-degree angle relative to the cavity and the signal is collected in cross-polarization, in order to remove the light reflected on top of the structure (not coupling to the cavity). Both methods are shown schematically in figure 2c. For both characterisation pathways the same device was measured and spectra of the cavity mode were collected.

For the PL configuration, a  $Q \sim 4272$  was measured at  $\sim 585$  nm, as shown in figure 2e. Employing the cross polarization method, a slightly lower  $Q$  of 3071 at  $\sim 583$  nm is observed, as shown in figure 2d. The measured  $Q$  using the PL method is slightly higher since the excitation and collection are focused at the cavity center, so the mode is captured with minimal losses. In the cross-polarization configuration, excitation goes through the grating couplers, which introduce scattering and coupling losses, and the signal passes through polarization optics. If the cavity mode's polarization isn't perfectly aligned with the analyzer, this can distort the mode and broaden the resonance.

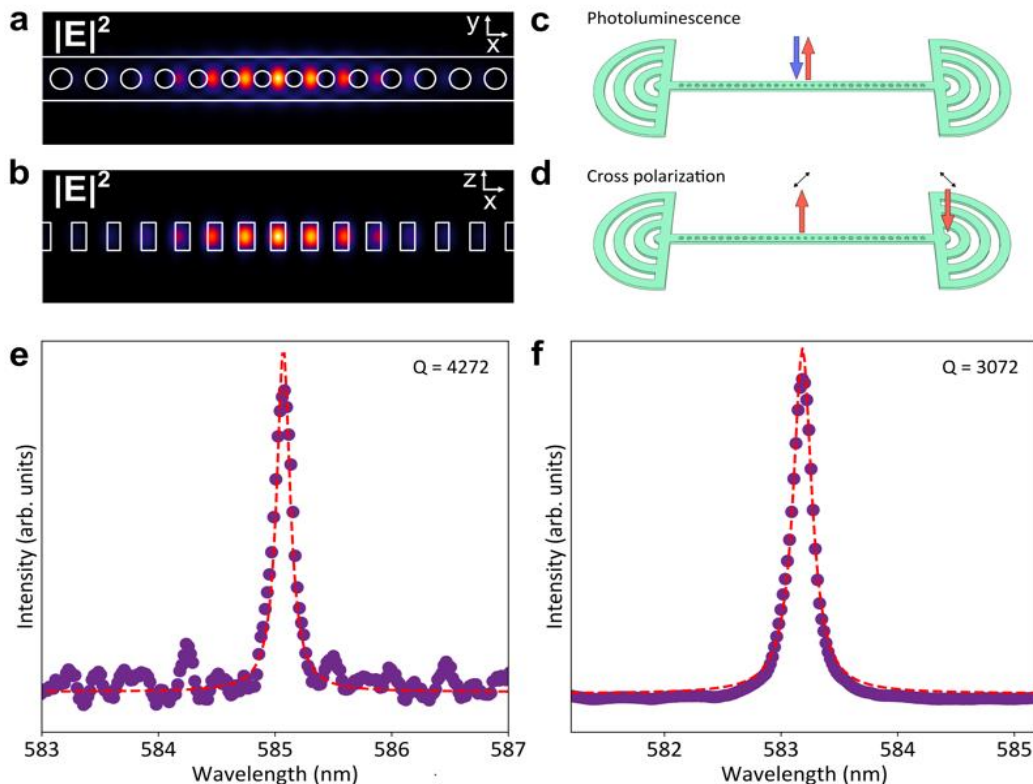


**Figure 2.** Characterisation of the 1D PCC resonant modes. a,b) FDTD simulations of the 1D PCC resonant mode at 577 nm in the XY (a) and XZ (b) planes. The mode is confined to the

center of the cavity. c) Schematic showing the collection and excitation pathways to characterise the cavity modes employing standard photoluminescence (PL) and d) resonant cross polarization technique using grating couplers. The arrows indicate the polarization of the input and output pathways. e) PL spectrum of the highest Q mode measured from a 1D PCC, with a  $Q \sim 4272$ . f) Same cavity mode as in (e), measured using the cross polarization configuration, resulting in a  $Q$  of 3071.

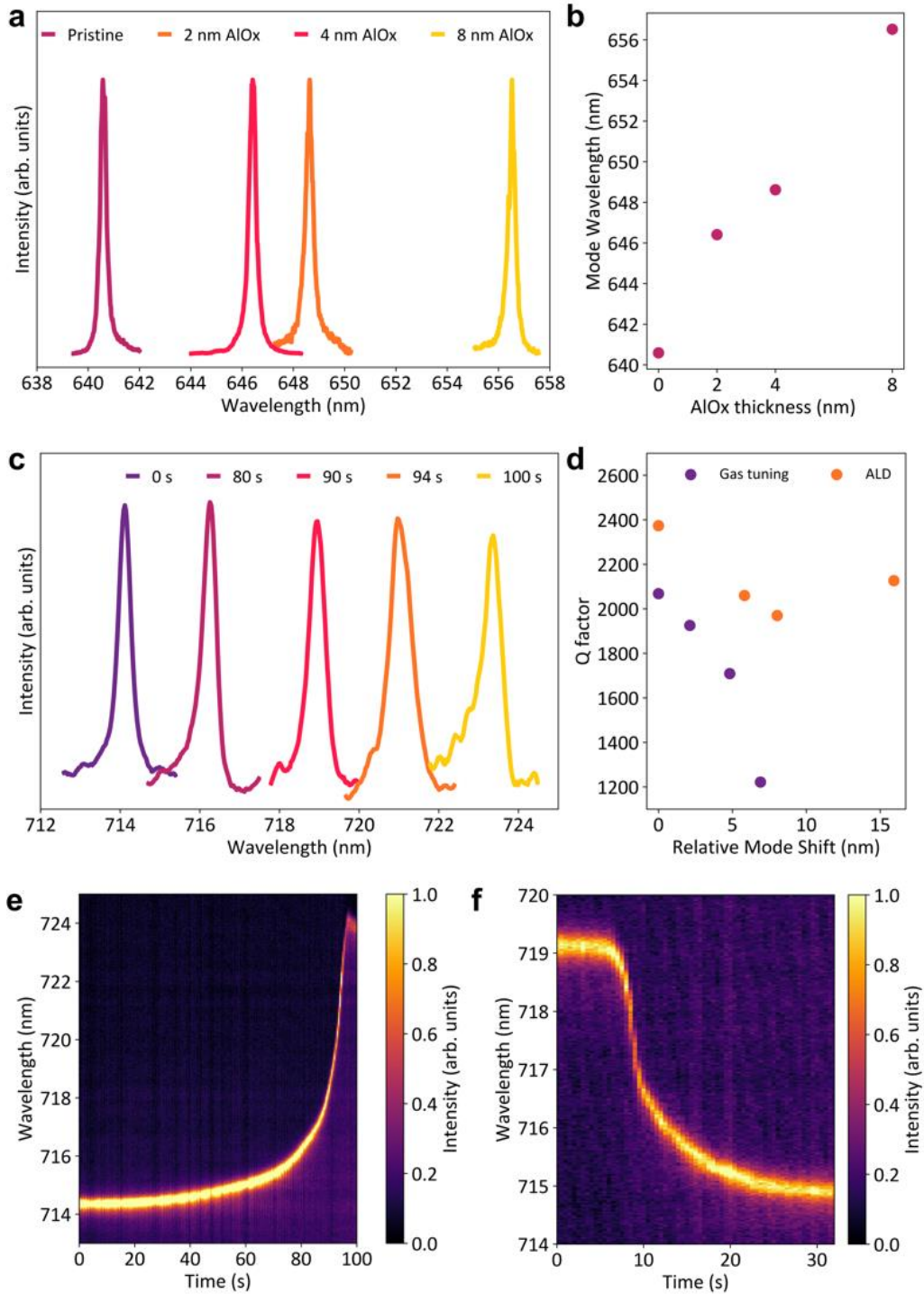
We now turn our attention to a controllable tuning of the cavity resonances. We implement two distinct approaches - namely gas condensation that modifies the cavity resonance due to change in refractive index, and ALD deposition that induces both refractive index change and increases cavity physical thickness. We use ALD to deposit a few nm of aluminium oxide (AlO) on top of the cavity. After each run, the devices were measured using the cross polarized method as it results in a better signal to noise ratio.

Figure 3a shows the experimental results. The cavity resonance is red shifted after each deposition of AlO<sub>x</sub> (2 nm, 4 nm, 8 nm). As expected, a linear trend in red shifted signal is observed, with the increased thickness of AlO<sub>x</sub> as shown in figure 3b. Overall, we achieved a tuning range of  $\sim 16$  nm without a significant degradation in the cavity quality factor (figure 3d, orange circles). Practically, high resolution cavity tuning of  $\sim 1$  nm is possible employing this method by depositing sub nm AlO<sub>x</sub> films with ALD.

The second cavity resonance tuning approach attempted was employing a gas condensation. Here we loaded the 1D PCC into a cryostat, which was cooled down to 8K. This measurement was conducted using the cross polarization set up. We chose nitrogen as the condensation gas, and it was flown at a rate of 5 standard cubic centimeters per minute (sccm). During the flow, cavity resonances were recorded (each measurement took  $\sim 1$  second). The cavity resonances then red shifted from  $\sim 714$  nm to  $\sim 723$  over  $\sim 100$  seconds, as shown in figure 3c. The mode profile broadened significantly as the mode red shifted, associated with a reduced quality factor.

The measured cavity quality factor,  $Q$ , as a function of tuning mechanism and duration are plotted in figure 3d. For the ALD method,  $Q$  remained relatively stable, without an obvious reduction. On the other hand, upon the gas condensation,  $Q$  degraded a lot, most likely due to the ice condensation on the cavity and an increased absorption and distortion in the cavity's physical geometry.

The full dynamic tuning range of the cavity modes - both red shift (condensation) and blue shift (evaporation) are shown in figure 3 (e, f). Initially the cavity mode shift is slow, most likely due to a delay between opening the mass flow controller and the gas entering the cryostat. The cavity mode at  $\sim 714$  nm, then rapidly shifts towards a maximum wavelength of  $\sim 723$  nm, representing a total shift of  $\sim 9$  nm. The appeal of using gas condensation is the ease at which the cavity resonance can then be blue shifted back to its original resonance. This is achieved by sublimation of the ice through the introduction of a second laser. This laser is focused on the centre of the cavity, which warms it up and melts the condensate. Once all the ice has been removed the cavity mode is tuned back to the initial wavelength.



**Figure 3.** Cavity mode tuning methods for 1D PCCs. **a)** Cross polarization spectra from the same 1D PCC showing the resonant cavity mode before (pristine) and after ALD deposition of  $\text{AlO}_x$  (2 nm, 4 nm, and 8 nm, respectively). **b)** Shift in the cavity resonance as a function of  $\text{AlO}_x$  thickness. **c)** Cross polarization spectra of a 1D PCC cavity mode tuned by a nitrogen gas condensation at 8K. The cavity mode is shown at different times as indicated in the figure. **d)** Measured cavity Q as a function of the spectral tuning from the initial cavity resonance for both ALD and gas tuning methods. **e)** Dynamic mode tuning of the 1D PCC in (c) by condensation, resulting in a red shift, and by sublimation (f), resulting in a blue spectral shift.

We now turn our attention into tuning the WGMs of the microdisk resonators. High resolution SEM image of the microdisk, overlaid with FDTD modelling of the WGMs, is shown in figure 4a. The light region at the centre of the microdisk resonator is the pedestal, where the microdisk is connected to the silicon substrate below. To tune the cavity resonances of the microdisk, we implemented the ALD method. Figure 4b shows the WGMs recorded from this microdisk with a  $Q \sim 2800$  at 635 nm and free spectral range (FSR) of  $\sim 14$  nm (purple curve). Upon deposition of  $\text{AlO}_x$  the WGMs are red shifted. As we repeat the process with 2 nm, 4 nm, 8 nm and 20 nm of  $\text{AlO}_x$ , we achieve a full spectral range (as shown in figure 4b). That means that the original WGM (indicated by the star), reaches the spectral location of the next WGM. Figure 4c displays the relationship between the amount of deposited  $\text{AlO}_x$  to the WGM wavelength, exhibiting a linear trend.

Finally, we showcase the high  $Q$  observed at the blue spectral range, where the most promising quantum emitters in hBN are emitting<sup>35, 36</sup>. Figure 4c shows the WGMs recorded from a 5  $\mu\text{m}$  diameter hBN microdisk, all exhibit  $Q$ s exceeding 2800 (SI figure SX). The highest measured  $Q$  from this device was  $Q \sim 8286$  at 460nm, as shown in figure 4e.

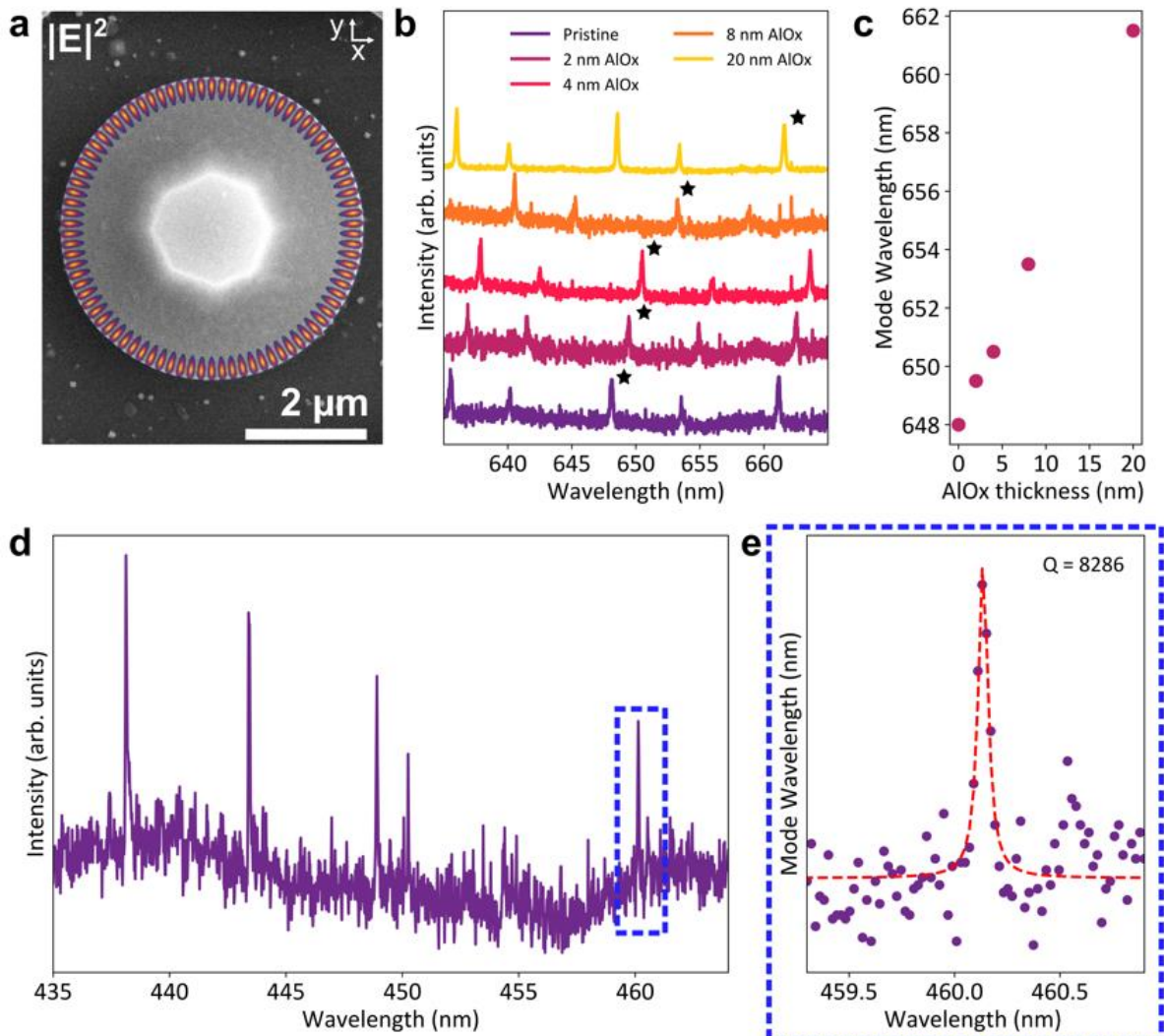


**Figure 4.** Microdisk cavity resonances and tuning. a) SEM image of the hBN microdisk cavity with a superimposed FDTD simulation of the mode profile at 457 nm. b) PL measurement of the WGMs from the same microdisk, showing the spectra before (pristine) and after ALD

deposition of  $\text{AlO}_x$  (2, 4, 8 and 20 nm). The spectra have been offset vertically for clarity. c) Shift in the cavity resonance as a function of  $\text{AlO}_x$  thickness. d) WGMs of an hBN microdisk at the blue spectral range. e) Cavity mode highlighted in blue rectangle in (d) with a measured  $Q \sim 8282$ .

A key aspect of the present work is the ability to reliably and controllably undercut the devices, thus enabling high Q cavities, specifically high Q WGMs in hBN microdisks. Earlier attempts of hBN device fabrication have almost exclusively used polymer hard masks for ICP-RIE processes - similarly to the method used in our work <sup>37, 38</sup>. However, recently, a double etch method employing a metal mask (chromium or nickel) has been proposed and demonstrated <sup>39, 40</sup>. This resulted in smoother side walls of the etched hBN nanostructures. However, we found that this method isn't optimal for undercutting the underlying substrate. The undercutting of 1D PCCs (or microdisk cavities) that were fabricated with a polymer mask takes approximately 12 minutes, when using 20% concentration KOH heated to 40°C. In comparison we found that when using either a chromium or nickel double etch process, no clear undercut is achieved even after doubling or tripling the undercutting time. Raising temperature or bubbling the KOH is not ideal for hBN either, since the flakes can disassociate from the substrate. A selection of parameters used to undercut metal masked devices are stated in the SI in table S1. Our results therefore suggest that if undercutting is required (i.e. for photonic cavities), polymer mask is preferred. However, when devices can sit on a substrate (i.e. metasurfaces or waveguides), metal mask can be used instead.

To conclude, we have successfully fabricated high quality photonic devices in hBN - specifically 1D PCCs and microdisk resonators. Through implementing a robust undercutting protocol, we achieved a record high Q from a monolithic hBN device in the blue spectral region, with qualities exceeding  $Q \sim 8,000$ . Further, we demonstrated two complementary cavity tuning mechanisms - gas condensation and ALD deposition - that can be readily implemented to tune cavity resonances in hBN. With the current focus on studying coherent properties of quantum emitters in blue spectral range, and the demonstrated here robust cavity engineering and tuning, we envision a promising pathway for a realisation of integrated quantum photonic circuitry with hBN.

## Acknowledgments

The authors acknowledge financial support from the Australian Research Council (CE200100010, FT220100053, DP250100973) the Air Force Office of Scientific Research (FA2386-25-1-4044). The authors thank Giorgio Gemisis for useful discussion. The authors thank the ANFF node at USYD and UTS for access to facilities.

## Methods

### Fabrication

hBN was exfoliated onto cleaned silicon substrates using scotch tape. Following this the samples were annealed in an STF1200 Tube Furnace. The tube furnace was programmed to ramp to 500°C over 3 hrs where it remained for 4hrs, then to ramped to 650°C over 1 hr

where it remained for 2 hrs then finally ramping to 820°C over 40 minutes where it remained for 40 minutes and then cooled down to ambient temperature over 6 hrs.

The samples were spin coated with an electron beam resist (CSAR.62 13) at 5K RPM for 60 seconds, and were then baked for 180 seconds at 180°C. The pattern was defined using electron beam lithography using an Elionix ELS-F125 for the 1D PCCs and a Helios G4 PFIB UXe DualBeam for the microdisk resonators . The pattern was developed by submerging the sample in CSAR developer 600-51, xylene and IPA for 60, 5 and 20 seconds respectively. A brief plasma cleaning step was conducted to remove residual polymer in the developed regions using a Trion inductively coupled plasma reactive ion etching (ICP-RIE) using the following parameters; 12 sccm oxygen, 10W ICP, 40W RIE, under 6 mTorr of pressure for 3 seconds.

Following this the pattern was transferred into the hBN in the same machine with the following parameters; 60 sccm Ar, 5 sccm SF6, 300W RIE under 10 mTorr of pressure. The residual CSAR was removed by submerging the sample in CSAR remover preheated to 135°C for one hour. Then rinsed in water and IPA before being blow dried using nitrogen.

For undercutting the silicon, the sample is submerged into 20% concentration potassium hydroxide preheated to 40°C for ~12 minutes to undercut both the 1D PCCs and microdisk resonators. Following this the devices were submerged in water and then IPA before being blow dried with nitrogen. Following this the device fabrication was completed.

### Photoluminescence

Photoluminescent (PL) measurements were conducted on a home-built confocal microscope set up with a 532 nm continuous-wave laser excitation laser and a 100x objective (Nikon 0.9 NA). A 532 nm long-pass dichroic and 568 nm long-pass filter were used to eliminate any reflected laser into the collection. The collection and excitation position were overlapped in this configuration and positioned at the centre of the 1D PCCs, and on the edge of the microdisk resonators. Emission was collected using a spectrometer (Andor Kymera 328i) using the 1800 lines/mm grating.

Cross polarization measurements were conducted on a home-built optical set using a Fianium supercontinuum laser and a 100x objective (Nikon 0.9 NA). Emission was collected using a spectrometer (Andor Kymera 328i) using the 1800 lines/mm grating. In the collection excitation pathway a  $\lambda/4$  and  $\lambda/2$  waveplates were used, rotated to maximise photon extinction on the spectrometer. The collection and excitation positions were uncoupled, with the collection at the centre of the cavity and the excitation on the grating couplers.

1. Flamini, F.; Spagnolo, N.; Sciarrino, F. Reports on progress in physics *Photonic quantum information processing: a review* 82, 16001 (2019)
2. Awschalom, D. D., et al. Science *Challenges and opportunities for quantum information hardware* 390, 1004-1010 (2025)
3. Pirandola, S., et al. Nature photonics *Advances in photonic quantum sensing* 12, 724-733 (2018)
4. Couteau, C., et al. Nature reviews physics *Applications of single photons to quantum communication and computing* 5, 326-338 (2023)

5. Pelucchi, E., et al. *Nature reviews physics The potential and global outlook of integrated photonics for quantum technologies* 4, 194-208 (2022)
6. Wang, J.; Sciarrino, F.; Laing, A.; Thompson, M. G. *Nat. Photonics Integrated photonic quantum technologies* 14, 273-284 (2020)
7. Wan, N. H., et al. *Nature Large-scale integration of artificial atoms in hybrid photonic circuits* 583, 226-231 (2020)
8. Xiao, Z., et al. *Advanced optical materials Recent Progress in Silicon-Based Photonic Integrated Circuits and Emerging Applications* 11, (2023)
9. Pérez-López, D.; Torrijos-Morán, L. *Npj nanophotonics Large-scale photonic processors and their applications* 2, 32-9 (2025)
10. Xiang, C.; Jin, W.; Bowers, J. E. *Photonics research (Washington, DC) Silicon nitride passive and active photonic integrated circuits: trends and prospects* 10, A82-A96 (2022)
11. Baek, K., et al. *Advanced materials technologies Advanced Optical Integration Processes for Photonic-Integrated Circuit Packaging* 10, n/a (2025)
12. Hu, Y., et al. *Nat. Commun. Integrated lithium niobate photonic computing circuit based on efficient and high-speed electro-optic conversion* 16, 8178 (2025)
13. Islam, F., et al. *Nano letters Cavity-Enhanced Emission from a Silicon T Center* 24, 319-325 (2024)
14. Duan, Y.; Chen, K. C.; Englund, D. R.; Trusheim, M. E. *Optics express A vertically-loaded diamond microdisk resonator spin-photon interface* 29, 43082-43090 (2021)
15. Zhang, J. L., et al. *Optica Complete coherent control of silicon vacancies in diamond nanopillars containing single defect centers* 4, 1317-1321 (2017)
16. Komza, L., et al. *Optica Multiplexed color centers in a silicon photonic cavity array* 12, 1400-1405 (2025)
17. Masuda, T., et al. *Optics express Fiber-taper collected emission from NV centers in high-Q/V diamond microdisks* 32, 8172-8188 (2024)
18. Lukin, D. M., et al. *Physical review. X Two-Emitter Multimode Cavity Quantum Electrodynamics in Thin-Film Silicon Carbide Photonics* 13, 011005 (2023)
19. Tiranov, A., et al. *Science Collective super- and subradiant dynamics between distant optical quantum emitters* 379, 389-393 (2023)
20. Ding, S. W., et al. *Nature Communications High-Q cavity interface for color centers in thin film diamond* 15, 6358-8 (2024)
21. Kuruma, K., et al. *Applied physics letters Coupling of a single tin-vacancy center to a photonic crystal cavity in diamond* 118, (2021)
22. Dibos, A. M.; Raha, M.; Phenicie, C. M.; Thompson, J. D. *Phys. Rev. Lett. Atomic Source of Single Photons in the Telecom Band* 120, 243601 (2018)
23. Ourari, S., et al. *Nature (London) Indistinguishable telecom band photons from a single Er ion in the solid state* 620, 977-981 (2023)
24. Qian, C., et al. *Nano letters Unveiling the Zero-Phonon Line of the Boron Vacancy Center by Cavity-Enhanced Emission* 22, 5137-5142 (2022)
25. Caldwell, J. D., et al. *Nature reviews. Materials Photonics with hexagonal boron nitride* 4, 552-567 (2019)
26. Çakan, A., et al. *Adv. Opt. Mater. Quantum Optics Applications of Hexagonal Boron Nitride Defects* 13, 2402508 (2025)
27. Li, C., et al. *ACS Photonics Integration of hBN quantum emitters in monolithically fabricated waveguides* 8, 2966-2972 (2021)
28. Kühner, L., et al. *Adv. Mater. High-Q Nanophotonics over the Full Visible Spectrum Enabled by Hexagonal Boron Nitride Metasurfaces* 35, 2209688 (2023)
29. Zotev, P. G., et al. *Nat. Photonics Nanophotonics with multilayer van der Waals materials* 19, 788-802 (2025)
30. Sakib, M. A., et al. *Nano Lett. Purcell-Induced Bright Single Photon Emitters in Hexagonal Boron Nitride* 24, 12390-12397 (2024)
31. Mai, T. N. A., et al. *Adv. Func. Mater. Quantum Emitters in Hexagonal Boron Nitride: Principles, Engineering and Applications* n/a, 2500714 (2025)

32. Kianinia, M.; Xu, Z.-Q.; Toth, M.; Aharonovich, I. J. A. P. R. *Quantum emitters in 2D materials: Emitter engineering, photophysics, and integration in photonic nanostructures* 9, 011306 (2022)
33. Nonahal, M., et al. *Laser & photonics reviews Engineering Quantum Nanophotonic Components from Hexagonal Boron Nitride* 17, n/a (2023)
34. Rah, Y.; Jin, Y.; Kim, S.; Yu, K. *Opt. Lett. Optical analysis of the refractive index and birefringence of hexagonal boron nitride from the visible to near-infrared* 44, 3797-3800 (2019)
35. Fournier, C., et al. *Physical review applied Two-Photon Interference from a Quantum Emitter in Hexagonal Boron Nitride* 19, (2023)
36. Horder, J., et al. *ACS photonics Optical Coherence of B Center Quantum Emitters in Hexagonal Boron Nitride* 12, 1284-1290 (2025)
37. Agarwal, H., et al. *JPhys materials In situ engineering hexagonal boron nitride in van der Waals heterostructures with selective SF6 etching* 8, 045006 (2025)
38. Nonahal, M., et al. *Nano letters Deterministic Fabrication of a Coupled Cavity–Emitter System in Hexagonal Boron Nitride* 23, 6645-6650 (2023)
39. Biechteler, J., et al. *Advanced optical materials Fabrication Optimization of van der Waals Metasurfaces: Inverse Patterning Boosts Resonance Quality Factor* 13, n/a (2025)
40. Schaeper, O. C., et al. *ACS photonics Double Etch Method for the Fabrication of Nanophotonic Devices from van der Waals Materials* 11, 5446-5452 (2024)